Surface Roughness Effects on Flow Boiling in Microchannels

Benjamin J. Jones

Suresh V. Garimella[1]
e-mail: sureshg@purdue.edu

NSF Cooling Technologies Research Center,
School of Mechanical Engineering,
and Birck Nanotechnology Center,
Purdue University,
585 Purdue Mall,
West Lafayette, IN 47907-2088

*The influence of surface roughness on flow boiling heat transfer and pressure drop in microchannels is experimentally explored. The microchannel heat sink employed in the study consists of ten parallel, 25.4 mm long channels with nominal dimensions of 500 $\times 500$ μm^2. The channels were produced by saw-cutting. Two of the test piece surfaces were roughened to varying degrees with electrical discharge machining (EDM). The roughness average R_a varied from 1.4 μm for the as-fabricated, saw-cut surface to 3.9 μm and 6.7 μm for the two roughened EDM surfaces. Deionized water was used as the working fluid. The experiments indicate that the surface roughness has little influence on boiling incipience and only a minor impact on saturated boiling heat transfer coefficients at lower heat fluxes. For wall heat fluxes above 1500 kW/m^2, the two EDM surfaces (3.9 μm and 6.7 μm) have similar heat transfer coefficients that were 20–35% higher than those measured for the saw-cut surface (1.4 μm). A modified Bertsch et al. [2009, "A Composite Heat Transfer Correlation for Saturated Flow Boiling in Small Channels," Int. J. Heat Mass Transfer, **52**, pp. 2110–2118] correlation was found to provide acceptable predictions of the flow boiling heat transfer coefficient over the range of conditions tested. Analysis of the pressure drop measurements indicates that only the roughest surface (6.7 μm) has an adverse effect on the two-phase pressure drop.*
[DOI: 10.1115/1.4001804]

Keywords: flow boiling, microchannel, heat transfer, surface roughness

1 Introduction

It is well recognized that the limits of heat dissipation that can be managed by air-cooled heat sink technology, the primary means of cooling microprocessors, are at hand. If the current pace of development in the microelectronics industry is to be sustained, new and innovative cooling strategies are needed. Flow boiling in microchannel heat sinks is a prime contender for replacement of the air-cooled heat sink due to the very high heat transfer rates attainable with this technology. Over the last decade, much research has, therefore, been devoted toward better understanding flow boiling phenomena in microchannels. Recent experimental studies [1–4] have shed light on the influence of heat flux, mass flux, vapor quality, and channel dimensions on the flow boiling heat transfer coefficients. Improvements in the predictability of flow boiling in small channels have been supported by recent developments in models for both heat transfer [5,6] and pressure drop [7–9]. Despite the advancements in the state of understanding of microchannel flow boiling, several important factors influencing flow boiling in microchannel heat sinks have yet to be fully explored. In particular, and as will be the topic of this paper, a detailed study of the influence of surface roughness on flow boiling in microchannels has not been reported in literature to the authors' knowledge.

It has long been known that surface characteristics have a significant impact on nucleate boiling heat transfer. Numerous investigations have focused on developing methods of enhancing heat transfer rates for in-tube flow boiling. Although most prior studies have considered macroscale two-phase flow systems, more recently, researchers have begun exploring surface augmentation techniques in minichannels and microchannels. Ammerman and You [10,11] studied flow boiling in a minichannel and a microchannel with a microporous coated bottom wall. The microporous coated channels resulted in approximately 1.4 times greater heat transfer coefficients than uncoated channels for most test conditions considered. This level of enhancement was somewhat less than the 1.5–3 times greater heat transfer coefficients compared with smooth surfaces that have typically been reported in macroscale tubes with similar coatings [12,13].

Microchannels with microfabricated notches and cavities were explored by Zhang et al. [14], Kandlikar et al. [15], Koşar et al. [16,17], Kuo and co-workers [18–20], Jones and co-workers [21,22], and Pate et al. [23]. Although the augmented channels resulted in lower wall superheats at incipience than smooth surfaces [14,19], the influence of the augmentation on heat transfer rates in fully developed boiling has not been entirely conclusive. From the data of Zhang et al. [14], there appeared to be little benefit from the augmented surface on heat transfer coefficients. Kuo and Peles [19] found that the augmented surfaces resulted in higher heat transfer coefficients than a smooth surface at higher mass fluxes; however, lower heat transfer coefficients were observed at lower mass fluxes. From the studies in literature, thus far, it appears that the main benefit in using these augmented surfaces is the suppression of flow instabilities in microchannel heat sinks [15,20,22].

Although surface roughness produced using standard machining operations appears to have fallen out of favor as a surface enhancement technique in macroscale boiling [24], it is still recognized as an important factor influencing boiling heat transfer. Since different methods of manufacturing microchannels impart different levels of roughness on the channel surfaces, an understanding of its effect on flow boiling is needed. An experimental exploration of the influence of surface roughness in microchannel flow boiling is therefore warranted. In this study, experimental results on flow boiling heat transfer and pressure drop with deionized water using three microchannel heat sinks of varying surface roughness (R_a=1.4 μm, 3.9 μm, and 6.7 μm) are reported.

2 Experimental Setup

2.1 Experimental Test Facility. A diagram of the experimental flow facility is shown in Fig. 1. A differential pressure trans-

[1]Corresponding author.
Contributed by the Heat Transfer Division of ASME for publication in the JOURNAL OF THERMAL SCIENCE AND ENGINEERING APPLICATIONS. Manuscript received May 18, 2009; final manuscript received February 26, 2010; published online June 24, 2010. Assoc. Editor: Anthony M. Jacobi.

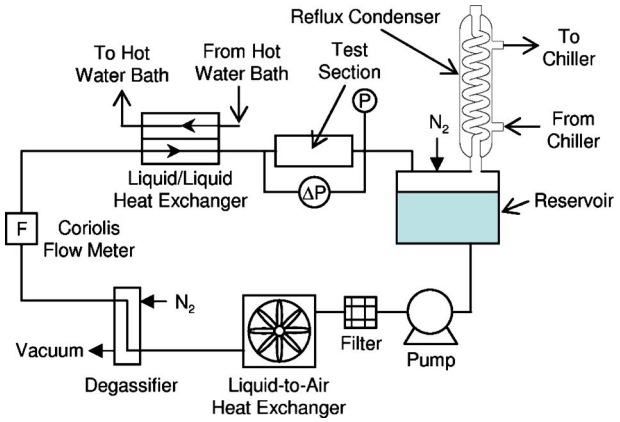

Fig. 1 Experimental flow loop

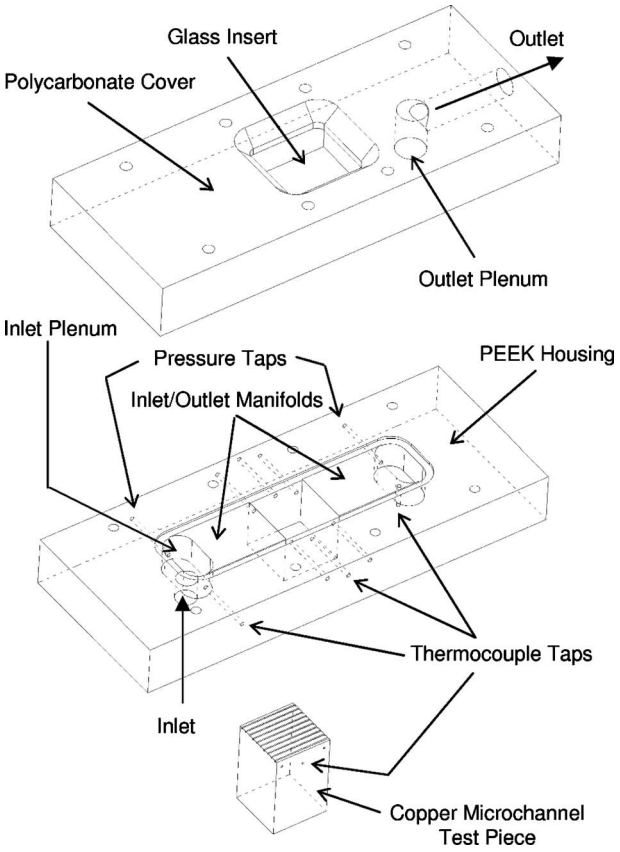

Fig. 2 Schematic of experimental test section

ducer is used to measure the pressure drop across the test section and a pressure transducer at the outlet measures gauge pressure. The outlet pressure transducer has an uncertainty of ± 0.31 kPa while the differential pressure transducer has an experimental uncertainty of ± 0.43 kPa. Inlet pressure measurements are calculated based on the differential pressure transducer and the outlet pressure transducer readings and, therefore, have an uncertainty of ± 0.53 kPa.

Subcooled liquid enters the microchannel test section. The subcooled liquid is maintained at the desired temperature using a liquid-to-liquid heat exchanger in conjunction with a large, temperature controlled, hot water bath circulation unit. The liquid/vapor exiting the microchannel test section flows into a reservoir. The vapor is condensed in a glass reflux condenser, which exchanges heat from the vapor to cold water from a chilled water circulation unit. The condensate falls into the reservoir. The condenser is open to the atmosphere and due to the low pressure drop in the tubing of the flow loop, atmospheric pressure is maintained at the exit of the microchannels. The reservoir is vented with high purity nitrogen. The purpose of the vented nitrogen is to displace the dissolved oxygen in the water, which can contribute to corrosion of the copper test surfaces used in the experiments.

A gear pump is used for pumping the fluid. A 7 μm sintered filter element removes any particulates from the flow loop. A liquid-to-air heat exchanger cools the fluid to near-ambient temperatures prior to entering temperature-sensitive equipment in the flow loop. A high-accuracy Coriolis flow meter measures the mass flow rate in the test loop. A vacuum degassifying system is used to remove dissolved gases in the fluid, which can lead to premature bubble nucleation and affect the boiling performance [25,26]. The vacuum degassifier consists of a flow passage constructed out of a hydrophobic, porous membrane. Vacuum is applied to the outside of the flow passage while liquid water flows through it. The membrane is gas-permeable allowing the dissolved gases to be extracted from the liquid as vacuum is applied. The hydrophobic nature of the membrane prevents the liquid from passing through the membrane's porous structure. A nitrogen sweep gas is used to help displace some of the remaining dissolved oxygen in the water. This method of degassing was found to be very effective in removing dissolved oxygen from the liquid, producing dissolved oxygen levels of less than 0.1 ppm after approximately 1.5 h of degassing.

2.2 Experimental Test Section. A schematic diagram of the experimental test section is shown in Fig. 2. The experimental test piece consists of an oxygen-free copper test block with ten channels, each nominally 500 μm wide by 500 μm high by 25.4 mm long, manufactured into the top of the block. Six thermocouple taps are drilled into the copper block (at three different locations along the flow direction and at two different heights). T-type sheathed thermocouples with a sheath diameter of 0.8 mm were used. The thermocouples were referenced to a dry-block ice-point reference chamber. All thermocouples were calibrated using a dry-block thermocouple calibration unit. Since all thermocouples were calibrated against the same, stable temperature source and referenced against a uniform ice-point reference temperature, the estimated uncertainty in temperature differences measured by the thermocouples is $\pm 0.1^\circ$C. However, absolute errors in the calibration and reference source lead to an estimate of $\pm 0.3^\circ$C for absolute temperature measurements. The bottom channel wall temperature is determined by extrapolation of the temperature measurements. Using standard uncertainty analysis, the estimated uncertainty in the wall temperature ranges from approximately $\pm 0.4^\circ$C near boiling incipience to $\pm 1.3^\circ$C at the maximum heat flux obtained in the experiments. Twelve cartridge heaters, inserted into holes drilled in the bottom of the test piece, supply the desired power input. The test piece is inserted into a polyetheretherketone (PEEK) (a thermoplastic with good resistance to high temperatures) housing. The cover of the test section is manufactured out of polycarbonate with a glass insert in contact with the top of the copper test block. Manifold and plenum regions were machined in the PEEK housing and polycarbonate cover to distribute fluid to and from the microchannels. Thermocouple and pressure taps in the inlet and outlet plenums of the PEEK housing allow measurement of the fluid inlet and outlet temperature and pressure drop across the test section. The lower portion of the copper microchannel test piece is enclosed in an alumina silicate ceramic shell for insulation (not shown in Fig. 2).

2.3 Microchannel Test Surfaces. Three microchannel test surfaces of varying surface roughness were fabricated into test pieces. The channels for one test piece were fabricated using a saw blade. The channels for the two other test pieces were roughened using electrical discharge machining (EDM). Different EDM

Table 1 Test piece characteristics and test conditions. Surface roughness values indicate mean±standard deviation.

	Channel dimensions		Surface roughness parameters				Experimental conditions		
Surface preparation	W_c (μm)	H_c (μm)	R_a (μm)	R_q (μm)	R_p (μm)	R_z (μm)	$T_{l,\text{in}}$ (°C)	G (kg/m^2 s)	Max. x_{out} (%)
Saw-cut	521	496	1.4	1.8	12	18	87.3	199	46.4
			±0.1	±0.1	±4	±4	86.9	609	24.0
							86.8	998	15.4
EDM	458	462	3.9	4.9	18	39	87.2	193	44.7
			±0.3	±0.3	±2	±2	87.0	604	29.5
							87.0	997	19.0
	510	480	6.7	8.4	34	58	87.1	203	36.5
			±0.4	±0.5	±3	±4	86.4	600	25.6
							86.6	994	16.4

parameters were used to vary the surface roughness between the two test pieces. These latter channels were first cut with a saw blade to undersized dimensions before undergoing the EDM roughening process. Enough material was removed with the EDM machining process to ensure that the final roughness had no residual features from the saw-cutting operation. It should be noted that the EDM process roughens all three heated sides of the copper microchannel surface.

Ram-type EDM, as opposed to wire EDM, was chosen due to its ability to produce channels with a form that more closely matches the shape of the channels produced with saw-cutting. A graphite electrode was fabricated for the EDM cutting process. The different EDM parameters used in roughening the two test pieces necessitated a different set of electrodes for each test piece in order to produce channels of similar widths since the amount of overburn (the gap between the electrode surface and the resulting machined surface) changed with the EDM parameter adjustment. During the EDM roughening process, the corners of the electrodes tend to wear preferentially resulting in a channel with rounded corners. This required periodic replacement of the electrodes with a new set in order to reduce the amount of corner-rounding. However, the fixed overburn distance over the periphery of the electrode leads to some corner-rounding being inevitable with EDM.

A black layer was formed on the electrical discharge machined copper surfaces. The exact nature of the black layer was not precisely known but is believed to be a carbon residue, perhaps deposited from the graphite electrode or EDM bath fluid products. Since the surface wettability was likely to be affected by such a layer, it was desirable to remove the layer and expose the bare copper surface prior to testing. Most of the layer could be removed by cleaning the test piece with deionized water in an ultrasonic bath for approximately 2 h. The remainder of the layer was removed using a weak copper etchant solution to etch the underlying copper and lift off the black residue. The copper test pieces were placed in an ultrasonic bath containing 0.3% hydrogen peroxide and 1% sulfuric acid solution. Approximately 20 min of ultrasonic agitation with the acid solution were required to completely remove the remaining residue.

2.4 Microchannel Characterization. The channel widths were measured using an optical microscope with a digital micrometer stage while the channel depths were measured with a Zygo NewView 7300 optical profiling system based on white light, vertical scanning interferometry. The optical profiling system was also used to measure the surface roughness of the bottom channel surfaces. The channel dimensions were measured at approximately 30 locations distributed across the microchannel heat sink while the surface profilometry was performed at 16 different locations. The average channel dimensions and surface roughness measurements for each test piece are shown in Table 1. The estimated uncertainty in the channel dimension measurements is 5 μm. The average channel dimensions are within ±10% of the nominal 500 μm by 500 μm for each test piece. Several surface roughness parameters are provided in Table 1, according to ASME B46.1-1995. For the remainder of this paper, R_a will be used to denote the roughness of the different surfaces. The surface topography of the bottom channel walls, as measured by the optical profiling system is shown in Fig. 3. The saw-cut operation produces a channel with a series of grooves (see Fig. 3(*a*)). The EDM operation produces an irregular pattern of cavities on the surface. The R_a=6.7 μm EDM surface (as seen in Fig. 3(*c*)) appears to have larger cavities than the R_a=3.9 μm surface (shown in Fig. 3(*b*)).

Representative profiles of the bottom channel wall are shown in Fig. 4. These profiles were obtained from the optical profilometer measurements by averaging the surface height along the flow direction of the channel. It is evident that the saw-cut operation produces a channel with a rather flat bottom wall (see Fig. 4(*a*)). The channel profiles were nearly square as intended. For the EDM channels, the profile is slightly more rounded, as is particularly evident in the R_a=6.7 μm surface (see Figs. 4(*b*) and 4(*c*)). As discussed in the previous subsection, although attempts were made to produce a channel cross section that was as square as possible, some rounding of the bottom wall did occur.

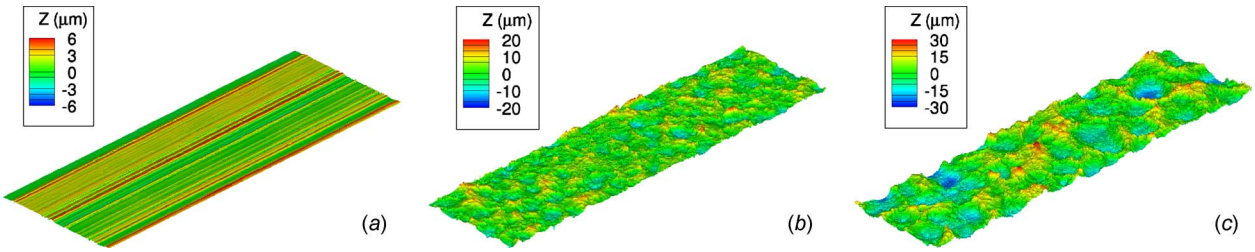

Fig. 3 Topographies of bottom channel surface

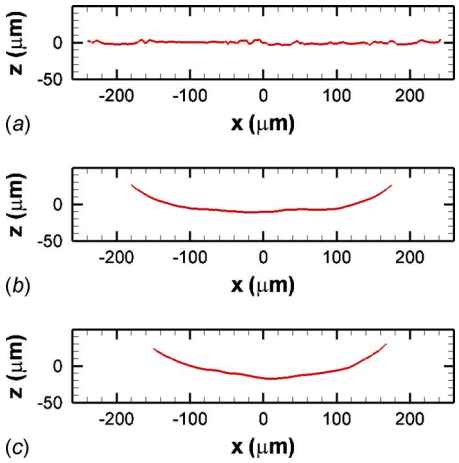

Fig. 4 Profiles of bottom channel surface

3 Data Reduction

3.1 Heat Transfer. The rate of heat transfer to the fluid Q was calculated using the readings from the thermocouples embedded in the copper test piece. The effective wall heat flux can be defined as

$$q = \frac{Q}{A_w} \tag{1}$$

where

$$A_w = N_c(W_c + 2\eta H_c) \tag{2}$$

and η is the fin efficiency. Due to the very large fin thickness (about 2 mm) relative to the channel dimensions, the fin efficiency is close to 1 (estimated value is 0.99 for a heat transfer coefficient of 50,000 $\mathrm{W/m^2\,K}$). The estimated uncertainty in the wall heat flux measurements ranges from $\pm 22\%$ of the measured wall heat flux near boiling incipience to $\pm 12\%$ at higher heat fluxes.

Since water enters the microchannel at subcooled temperatures, the channel length can be partitioned into three regions.

$$L = L_{sp} + L_{sub} + L_{sat} \tag{3}$$

where L_{sp}, L_{sub}, and L_{sat} are the lengths of the single-phase, the subcooled boiling, and the saturated boiling regions, respectively. The point of zero thermodynamic quality defines the boundary between the subcooled and saturated boiling regions, assuming thermodynamic equilibrium between the liquid and vapor phases. The local thermodynamic quality can be defined as

$$x = \frac{i - i_{l,\mathrm{sat}}}{h_{fg}} \tag{4}$$

where i is the local enthalpy and $i_{l,\mathrm{sat}}$ is the liquid enthalpy evaluated at saturated conditions corresponding to the local pressure.

The length of the single-phase and subcooled boiling regimes can be determined from an energy balance.

$$L - L_{sat} = L_{sp} + L_{sub} = \frac{\dot{m}c_p(T_{sat,0} - T_{l,in})}{q(A_w/L)} \tag{5}$$

where $T_{sat,0}$ is the saturation temperature at $x=0$. Assuming that the local saturation temperature follows a linear relationship between the inlet and outlet of the microchannel as suggested by Collier [27], the length of the subcooled regions can also be expressed as

$$\frac{L_{sp} + L_{sub}}{L} = \frac{T_{sat,0} - T_{sat,in}}{T_{sat,out} - T_{sat,in}} \tag{6}$$

where $T_{sat,in}$ and $T_{sat,out}$ are the saturation temperatures evaluated based on the inlet and outlet pressure readings, respectively. Solving Eqs. (5) and (6) yields the lengths of the subcooled and saturated regions.

The saturated boiling heat transfer coefficient can then be calculated as

$$h_{sat} = \frac{q}{\bar{T}_w - \bar{T}_{sat}} \tag{7}$$

where $\bar{T}_w$ is the mean wall temperature and $\bar{T}_{sat}$ is the mean saturated fluid temperature in the saturated boiling region. The estimated uncertainty in the heat transfer coefficients ranges from $\pm 25\%$ at heat fluxes near boiling incipience to $\pm 13\%$ at higher heat fluxes.

3.2 Pressure Drop. The pressure taps are located upstream and downstream from the inlet and outlet of the microchannels, respectively, (see Fig. 2). Therefore, determination of the pressure drop across the microchannels ΔP_c requires correction of the measured pressure drop ΔP using estimates of the pressure losses in the manifolds and pressure losses/recoveries due to flow area changes. However, calculations revealed that the significant pressure corrections are only due to the contraction from the inlet manifold to the microchannels and the expansion from the channels to the outlet manifold. Therefore, the channel pressure drop can be calculated as

$$\Delta P_c = \Delta P - \Delta P_{con} + \Delta P_{exp} \tag{8}$$

The fluid enters the microchannels as subcooled, single-phase liquid. Therefore, the contraction losses at the inlet of the microchannel can be estimated from Ref. 28.

$$\Delta P_{con} = \left[1 - \left(\frac{N_c A_c}{A_{man}}\right)^2 + K_{con}\right]\left(\frac{G^2}{2\rho_l}\right) \tag{9}$$

where

$$K_{con} = 0.0088\alpha^2 - 0.1785\alpha + 1.6027 \tag{10}$$

The pressure recovery due to flow expansion at the exit of the microchannel depends on whether there is single-phase or two-phase flow at this location. For a thermodynamic exit quality of $x_{out} < 0$, single-phase flow is assumed while two-phase is assumed for $x_{out} > 0$. For single-phase flow, the pressure recovery can be expressed as [28]

$$\Delta P_{exp} = \frac{1}{2\rho_l} K_{exp} G^2 \tag{11}$$

where

$$K_{exp} = 2.66\left(\frac{N_c A_c}{A_{man}}\right)\left(1 - \frac{N_c A_c}{A_{man}}\right) \tag{12}$$

For two-phase flow, the pressure recovery due to expansion is given by [29]

$$\Delta P_{exp} = \frac{1}{2\rho_l} K_{exp} G^2 (1 - x_{out})^2 \phi_l^2 \tag{13}$$

where K_{exp} for two-phase flow will be taken as [28]

$$K_{exp} = 2\left(\frac{N_c A_c}{A_{man}}\right)\left(1 - \frac{N_c A_c}{A_{man}}\right) \tag{14}$$

The two-phase friction multiplier ϕ_l is calculated using the Mishima and Hibiki [30] correlation.

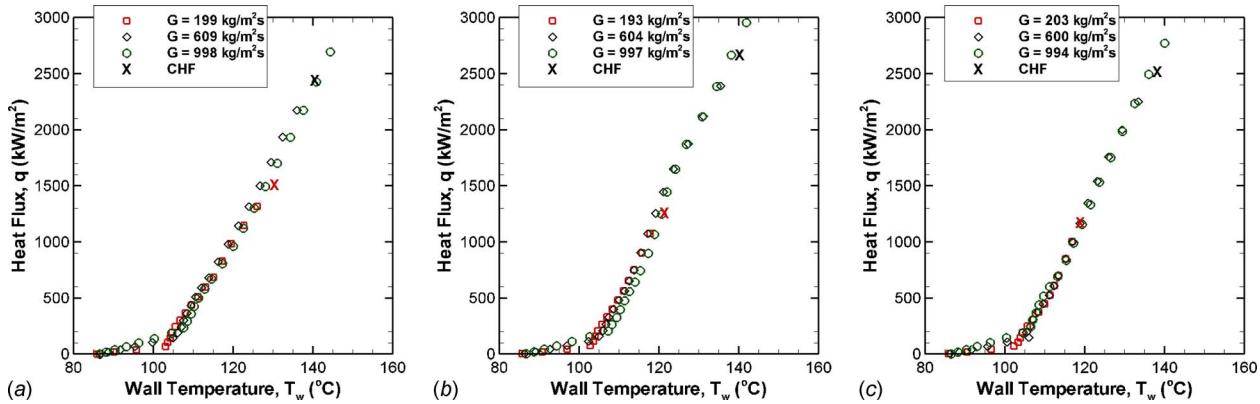

Fig. 5 Flow boiling curves for different surface conditions at different mass fluxes

$$\phi_l^2 = 1 + \frac{C}{X} + \frac{1}{X^2} \tag{15}$$

where

$$C = 21[1 - \exp(-319D_h)] \tag{16}$$

where D_h is in meters. The Martinelli parameter depends on whether the liquid and vapor phases are in the laminar or turbulent regimes. For the current set of experiments, most of the data fall in the viscous-liquid, viscous-vapor regime. However, the vapor Reynolds number is sufficient in some instances for turbulent-vapor conditions. The Martinelli parameter is calculated as [31]

$$X_{vv}^2 = \left(\frac{1-x}{x}\right)\left(\frac{\rho_v}{\rho_l}\right)\left(\frac{\mu_l}{\mu_v}\right); \quad \begin{matrix}\mathrm{Re}_l < 2000 \\ \mathrm{Re}_v < 2000\end{matrix} \tag{17}$$

$$X_{vt}^2 = 348\ \mathrm{Re}_v^{-0.8}\left(\frac{1-x}{x}\right)\left(\frac{\rho_v}{\rho_l}\right)\left(\frac{\mu_l}{\mu_v}\right); \quad \begin{matrix}\mathrm{Re}_l < 2000 \\ \mathrm{Re}_v > 2000\end{matrix} \tag{18}$$

4 Results and Discussion

4.1 Heat Transfer Results. The experimental conditions are reported in Table 1. The inlet temperature of the test section was maintained at 87°C for all tests. Data were collected at three different mass fluxes for each experimental test piece: nominally 200 kg/m^2 s, 600 kg/m^2 s, and 1000 kg/m^2 s. Heat fluxes up to approximately 3000 kW/m^2 were achieved, although the heat flux was limited to lower values by critical heat flux in some of the tests. The calculated equilibrium thermodynamic exit quality x_{out} ranged from approximately 45% at the lowest mass flux (200 kg/m^2 s) to approximately 15% at the highest (1000 kg/m^2 s). The saw-cut and 3.9 μm EDM tests were conducted at a mass flux of 1000 kg/m^2 s numerous times to ensure repeatability of the results. For both test sections, the measured wall temperature was repeatable to within approximately 2°C.

The flow boiling curves for the R_a=1.4 μm, 3.9 μm, and 6.7 μm surfaces are shown in Figs. 5(*a*)–5(*c*), respectively. For low superheats, single-phase fluid flows through the entire microchannel. Boiling commences at wall superheats ranging from 2 K to 3 K for a mass flux of 200 kg/m^2 s and from 6 K to 8 K for a mass flux of 1000 kg/m^2 s. The requirement of higher wall superheats at the higher mass fluxes may be due to a larger temperature gradient being present in the near wall region, producing a thinner superheated liquid layer that suppresses nucleate boiling. The surface roughness does not appear to have a substantial effect on the wall superheat at incipience. Once boiling commences, a higher slope in the boiling curve compared with the single-phase region is apparent due to the higher heat transfer coefficients with boiling heat transfer. In the fully developed boiling region, mass flux does not appear to have a major influence on the boiling curve for the range of conditions tested. According to Lee and Mudawar [32], the influence of mass flux on boiling heat transfer is dependent on the experimental conditions; with some researchers, similar to the current study, finding a weak dependence [2,4,33] while others have reported a strong dependence [34,35].

Critical heat flux (CHF) was experimentally achieved in the G=200 kg/m^2 s and 600 kg/m^2 s cases. For the G=1000 kg/m^2 s cases, the maximum heat flux was limited by the power supply used in the experiments rather than CHF. The critical heat flux measurements are shown in Fig. 6. For the lower mass flux case (200 kg/m^2 s), the R_a=3.9 μm and 6.7 μm surfaces had an 18% and 22% lower CHF value than the saw-cut surface, respectively. At a mass flux of 600 kg/m^2 s, the 3.9 μm surface had a 9% higher CHF than the saw-cut one while the 6.7 μm surface had a nearly identical CHF value as the saw-cut surface. It should be noted that the precision with which the CHF values are determined is limited to the heat flux increment used in the experiments near CHF (150–250 kW/m^2). Nonetheless, it does not appear that the surface roughness has a large influence on the critical heat flux under the conditions tested.

The influence of surface roughness on the saturated boiling heat transfer coefficients can be seen in Figs. 7(*a*)–7(*c*) for mass fluxes of 200 kg/m^2 s, 600 kg/m^2 s, and 1000 kg/m^2 s, respectively. All mass fluxes showed a similar trend. For heat fluxes below approximately 700 kW/m^2, there does not appear to be a significant effect of surface roughness on the saturated boiling heat transfer coefficient. Although for G=1000 kg/m^2 s, the 6.7 μm surface does have notably higher heat transfer coefficients than

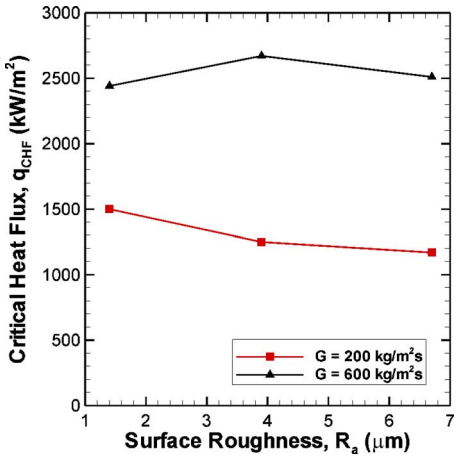

Fig. 6 Critical heat flux versus surface roughness at two different mass fluxes

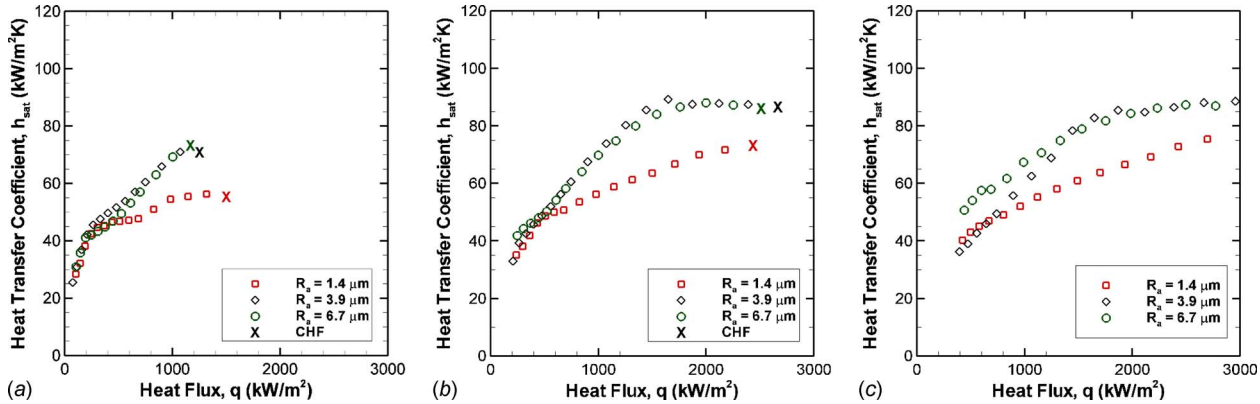

Fig. 7 Influence of surface roughness on saturated heat transfer coefficients at different mass fluxes

the other surfaces yet still within the estimated range of experimental uncertainty. At higher heat fluxes, the effect of surface roughness on the heat transfer coefficient is more marked. For heat fluxes above 1500 kW/m^2, the EDM surfaces have approximately 20–35% higher heat transfer coefficients than the saw-cut surface at a given heat flux. However, there is no significant difference in the measured heat transfer coefficients between the two EDM surfaces (3.9 μm and 6.7 μm surfaces) at these higher heat fluxes.

As discussed earlier (and as indicated in Table 1), the channel dimensions of the three test pieces vary by $\pm 10\%$ of the nominal 500×500 μm^2 channel dimensions. The experimental results of Harirchian and Garimella [2,4], using microchannels with dimensions ranging from 100×400 μm^2 ($W_c \times H_c$) to 5850×400 μm^2, indicate that saturated flow boiling heat transfer coefficients are not significantly influenced by small changes in channel dimensions. It is, therefore, believed that the differences in heat transfer coefficients measured in the current tests are a result of the different surface roughness rather than due to small differences in channel dimensions.

4.2 Heat Transfer Predictions. Bertsch et al. [36] compiled an extensive review of heat transfer correlations for saturated flow boiling in small channels. They found that the Cooper [37,38] pool boiling correlation outperformed most dedicated flow boiling correlations when evaluated against a large database of experimental results assembled from a wide range of studies in literature. The Cooper correlation resulted in mean absolute error (MAE) of 36% when compared with this large database. Bertsch et al. [5] later developed a composite model based on the formulation of Chen [39], offering improved predictions for flow boiling in small channels (MAE of 28% compared with the same database).

$$h_{FB} = h_{NB}(1-x) + h_{conv,tp}[1 - 80(x^2 - x^6)\exp(-0.6\mathrm{Co})] \quad (19)$$

where

$$h_{conv,tp} = h_{conv,l}(1-x) + h_{conv,v}x \quad (20)$$

The nucleate boiling heat transfer coefficient h_{NB} is evaluated from the Cooper [37,38] correlation (see Table 2) and the liquid and vapor convective heat transfer coefficients are evaluated from the Hausen [40] correlation. Since the Cooper correlation already includes a factor accounting for the effect of surface roughness, it is instructive to ascertain how well the Bertsch et al. flow boiling correlation (Eq. (19)) predicts saturated heat transfer coefficients over the wide range of surface roughness considered in the current study.

It should be noted that the experimentally determined saturated heat transfer coefficients presented in this study are averaged over a thermodynamic quality ranging from 0 to the channel exit quality x_{out} (Table 1 presents the maximum exit qualities obtained in the study) while the Bertsch et al. correlation (Eq. (19)) predicts heat transfer coefficients at a particular quality. Based on the definition of the saturated heat transfer coefficient in this study (Eq. (7)), an average flow boiling heat transfer coefficient can be calculated from a local heat transfer coefficient using

$$h_{FB,avg} = \frac{1}{\frac{1}{x_{out}}\int_0^{x_{out}} \frac{1}{h_{FB}(x)}dx} \quad (21)$$

Figure 8(a) presents the comparison between the Bertsch et al. correlation predictions (see Eq. (19)) and the experimental results. The predictions for water with the channel exit at atmospheric pressure deviate from the experimental results. The reason for this deviation is the unsuitability of the Cooper correlation at low reduced pressures. As described in Jones et al. [41], Cooper accounted for surface roughness by reformulating the Nishikawa and co-workers [42,43] relationship of $h \propto R_{p,old}^{(1-P_r)/5}$ into $h \propto P_r^{-0.2\log_{10} R_{p,old}}$. The reformulation provides a close approximation to the original formulation of Nishikawa et al. for reduced pressures above 0.08 or for a surface roughness near $R_{p,old} = 1$ μm but is unsuitable for lower reduced pressures when the roughness deviates from $R_{p,old} = 1$ μm.

For low reduced pressures, either the Gorenflo [44] nucleate boiling correlation or the Cooper [37,38] correlation reformulated to include the surface roughness factor originally proposed by Nishikawa et al. [42,43] should prove more suitable (see Table 2) for use in Eq. (19). It should be noted that such a modified Cooper correlation provides nearly identical predictions to the original formulation by Cooper for reduced pressures above 0.08. As indicated in Figs. 8(b) and 8(c), the Bertsch et al. correlation utilizing the Gorenflo or modified Cooper correlation offers much improved predictions with MAEs of 22.5% and 21.8%, respectively, and predicting 70% and 72% of the data within a deviation of $\pm 30\%$, respectively. Considering the expected errors of current

Table 2 Correlations for calculating nucleate boiling heat transfer coefficient h_{NB}

Author(s)	Correlation
Cooper [37,38]	$h = 55(P_r^{0.12-0.2\log_{10} R_{p,old}})(-\log_{10} P_r)^{-0.55} M^{-0.5} q^{0.67}$
Modified Cooper	$h = 55 P_r^{0.12} R_{p,old}^{(1-P_r)/5}(-\log_{10} P_r)^{-0.55} M^{-0.5} q^{0.67}$
	$\frac{h}{h_0} = \left[1.73 P_r^{0.27} + \left(6.1 + \frac{0.68}{1-P_r}\right)P_r^2\right] \times \left(\frac{R_a}{R_{a0}}\right)^{0.133}\left(\frac{q}{q_0}\right)^{0.9-0.3P_r^{0.15}}$
Gorenflo [44]	$q_0 = 20{,}000$ W/m^2, $h_0 = 5600$ W/m^2 K, $R_{a0} = 0.4$ μm

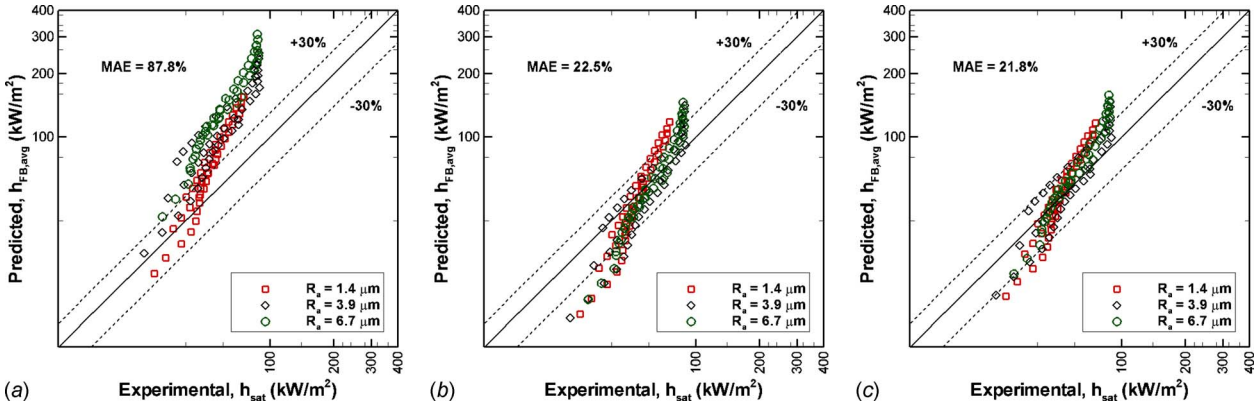

Fig. 8 Comparison of experimental measurements of saturated heat transfer coefficients with predictions

state-of-the-art flow boiling correlations, the modified Bertsch et al. correlations appear to offer acceptable predictions even over the range of surface roughness considered in this study. However, the reasons for the similar heat transfer characteristics of the R_a =3.9 and 6.7 μm surfaces are not adequately explained by the current models, which illustrates the general weakness in using R_a to characterize boiling surfaces. Improved methods of accounting for the surface roughness effect on flow boiling heat transfer are certainly desired.

4.3 Pressure Drop Results. The pressure drop results are shown in Fig. 9. At low heat fluxes in the single-phase regime, the pressure drop is independent of heat flux. Once boiling commences, the pressure drop increases with an increase in heat flux. Similar pressure drop values were measured for the two EDM surfaces (R_a=3.9 and 6.7 μm). In the saturated boiling regime, the pressure drop is on average 40% and 45% higher for the 3.9 μm and 6.7 μm surfaces, respectively, compared with the 1.4 μm surface. However, unlike the heat transfer coefficients, the differences in pressure drop are due to differences in the channel dimensions in addition to possible surface roughness effects. It is, therefore, necessary to gauge the influence of channel dimensions on the pressure drop before the surface roughness effect can be ascertained.

The influence of channel dimension can be estimated from two-phase pressure drop correlations available in literature. However, there is no general agreement on the most applicable pressure drop correlation to microchannels. Several small-channel correlations (such as those by Lee and Lee [45], Mishima and Hibiki [30], Mudawar and co-worker [7,8], and Lee and Garimella [9]) were compared for validation against the experimental results for the R_a=1.4 μm since this surface most closely matches the test pieces used in the development of the various previous pressure drop correlations. It was found that the Lee and Garimella [9] correlation provided the most accurate predictions of the measured pressure drop results for the current set of experiments. A comparison of the experimental pressure drop and the predictions from Lee and Garimella [9] is shown in Fig. 10. The predictions match the experimental data with a mean absolute error of 17.6% with 83% of the experimental data falling within ±30% of the predictions. Therefore, the Lee and Garimella [9] correlation is used to predict the influence of channel dimensions on pressure drop.

On average, the Lee and Garimella [9] correlation predicts that the 3.9 μm roughness channels should have approximately a 40% larger pressure drop than the 1.4 μm roughness channels due to the smaller channel dimensions (see Table 1) while the 6.7 μm surface is predicted to have approximately 20% larger pressure drop than the saw-cut channels. As previously noted, this compares to the experimental measurements of 40% and 45% larger pressure drops for 3.9 μm and 6.7 μm surfaces, respectively, compared with the saw-cut surface. Based on this analysis, it appears that the larger pressure drop of the 3.9 μm surface is due purely to smaller channel dimensions than the 1.4 μm surface. However, the increased roughness of the 6.7 μm surface does appear to have a noticeable adverse impact on the pressure drop.

5 Conclusions

Experiments were conducted on three microchannel heat sinks with different surface roughness (R_a=1.4 μm, 3.9 μm, and 6.7 μm). For the current test surfaces, roughness did not appear to have a significant impact on the boiling incipience wall temperature. Surface roughness was also found to have only a minor

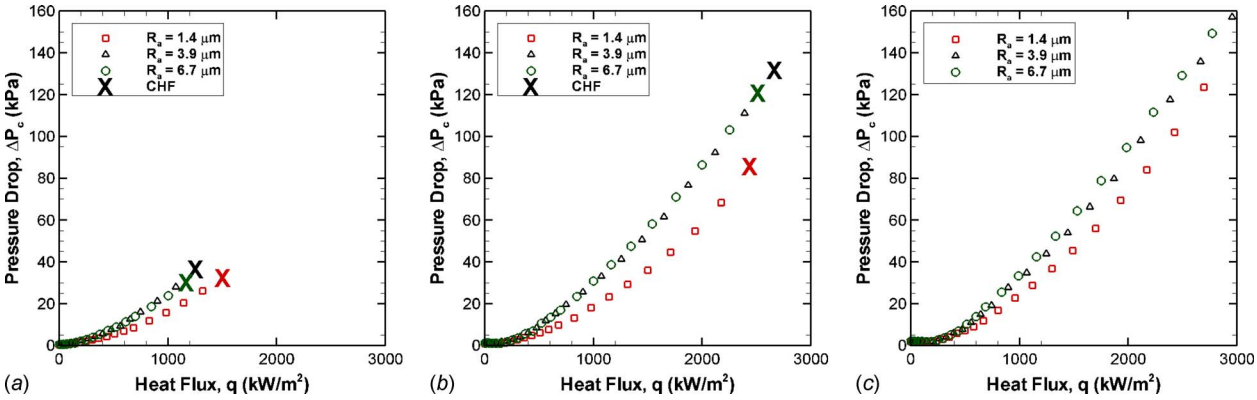

Fig. 9 Influence of surface roughness on channel pressure drop at different mass fluxes

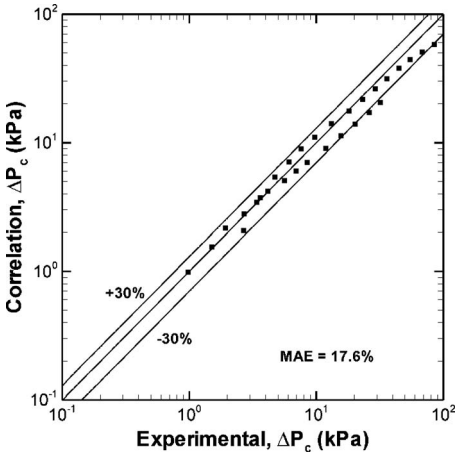

Fig. 10 Comparison of experimental pressure drop results to those of Lee and Garimella [9]

influence on the critical heat flux. For wall heat fluxes below 700 kW/m^2, only small differences in the saturated boiling heat transfer coefficient due to surface roughness were measured. However, at higher heat fluxes, the EDM surfaces (3.9 μm and 6.7 μm) have notably higher heat transfer coefficients than the saw-cut surface (1.4 μm) at a given heat flux. The two EDM surfaces have similar values for the heat transfer coefficients at higher heat fluxes. For a fixed heat flux above 1500 kW/m^2, the EDM surfaces have between 20% and 35% higher heat transfer coefficients than the saw-cut surface.

The Bertsch et al. [5] correlation from literature, modified for the low reduced pressures of the current study using the Gorenflo or modified Cooper correlation to predict the nucleate boiling heat transfer coefficient, provided acceptable flow boiling heat transfer predictions over the entire range of test conditions considered in the present study.

From analysis of the pressure drop measurements, it is not believed that the 3.9 μm surface causes a measurable increase in the pressure drop. However, the 6.7 μm surface does appear to have an adverse effect on the pressure drop compared with the 1.4 μm and 3.9 μm surfaces. The results of this experimental study demonstrate that under certain conditions, surface roughness can have a notable influence on heat transfer and pressure drop in microchannel flow boiling and therefore is an important parameter for consideration when designing microchannel heat sinks.

Acknowledgment

Dr. Dong Liu, Dr. Tailian Chen, and Dr. Poh-Seng Lee are thanked for their helpful and insightful discussions. Financial support from the Indiana 21st Century Research and Technology Fund and the Cooling Technologies Research Center, an NSF IUCRC at Purdue University, is gratefully acknowledged.

Nomenclature

A = area
Co = confinement number, $\mathrm{Co}=\sqrt{\sigma/(g(\rho_l-\rho_v)D_h^2)}$
c_p = specific heat
D_h = hydraulic diameter
G = mass flux
g = acceleration of gravity
H_c = channel height
h = heat transfer coefficient
h_{fg} = heat of vaporization
i = enthalpy
K = pressure loss coefficient
L = length
M = molecular weight
$\dot{m}$ = mass flow rate
N_c = number of channels
P = pressure
q = wall heat flux
R_a, R_q, R_z, R_p = roughness parameters according to ASME B46.1-1995
$R_{p,\mathrm{old}}$ = "Glättungstiefe" according to DIN 4762/1:1960, $R_{p,\mathrm{old}}\approx 0.4R_a$ [44]
Re_l = Reynolds number if liquid flows alone, $\mathrm{Re}_l=G(1-x)D_h/\mu_l$
Re_v = Reynolds number if vapor flows alone, $\mathrm{Re}_v=GxD_h/\mu_v$
T = temperature
W_c = channel width
X = Martinelli parameter
x = thermodynamic equilibrium quality

Greek

α = aspect ratio
η = fin efficiency
μ = dynamic viscosity
ρ = density
σ = surface tension
ϕ = two-phase friction multiplier

Subscripts

0 = value at a thermodynamic quality of $x=0$
avg = average
c = channel
con = contraction
CHF = critical heat flux
conv = convective
exp = expansion
FB = flow boiling
in = inlet
l = liquid
man = manifold
NB = nucleate boiling
out = outlet
r = reduced property
sat = saturated
sp = single-phase
sub = subcooled
tp = two-phase
v = vapor
vt = viscous liquid, turbulent vapor
vv = viscous liquid, viscous vapor
w = wall

References

[1] Bertsch, S. S., Groll, E. A., and Garimella, S. V., 2008, "Refrigerant Flow Boiling Heat Transfer in Parallel Microchannels as a Function of Local Vapor Quality," Int. J. Heat Mass Transfer, **51**, pp. 4775–4787.
[2] Harirchian, T., and Garimella, S. V., 2008, "Microchannel Size Effects on Local Flow Boiling Heat Transfer to a Dielectric Fluid," Int. J. Heat Mass Transfer, **51**, pp. 3724–3735.
[3] Bertsch, S. S., Groll, E. A., and Garimella, S. V., 2009, "Effects of Heat Flux, Mass Flux, Vapor Quality, and Saturation Temperature on Flow Boiling Heat Transfer in Microchannels," Int. J. Multiphase Flow, **35**, pp. 142–154.
[4] Harirchian, T., and Garimella, S. V., 2009, "Effects of Channel Dimension, Heat Flux, and Mass Flux on Flow Boiling Regimes in Microchannels," Int. J. Multiphase Flow, **35**, pp. 349–362.
[5] Bertsch, S. S., Groll, E. A., and Garimella, S. V., 2009, "A Composite Heat Transfer Correlation for Saturated Flow Boiling in Small Channels," Int. J. Heat Mass Transfer, **52**, pp. 2110–2118.
[6] Kandlikar, S. G., 1998, "Heat Transfer Characteristics in Partial Boiling, Fully Developed Boiling, and Significant Void Flow Regions of Subcooled Flow Boiling," ASME J. Heat Transfer, **120**, pp. 395–401.
[7] Qu, W., and Mudawar, I., 2003, "Measurement and Prediction of Pressure Drop in Two-Phase Micro-Channel Heat Sinks," Int. J. Heat Mass Transfer, **46**, pp. 2737–2753.
[8] Lee, J., and Mudawar, I., 2005, "Two-Phase Flow in High-Heat-Flux Micro-

Channel Heat Sink for Refrigeration Cooling Applications: Part I—Pressure Drop Characteristics," Int. J. Heat Mass Transfer, **48**, pp. 928–940.
[9] Lee, P.-S., and Garimella, S. V., 2008, "Saturated Flow Boiling Heat Transfer and Pressure Drop in Silicon Microchannel Arrays," Int. J. Heat Mass Transfer, **51**, pp. 789–806.
[10] Ammerman, C. N., and You, S. M., 1998, "Enhancing Small-Channel Convective Boiling Performance Using a Microporous Surface Coating," 1998 International Mechanical Engineering Congress and Exposition, Anaheim, CA, Vol. 3, pp. 467–476.
[11] Ammerman, C. N., and You, S. M., 2001, "Enhancing Small-Channel Convective Boiling Performance Using a Microporous Surface Coating," ASME J. Heat Transfer, **123**, pp. 976–983.
[12] Kovalev, S. A., and Shklover, E. G., 1988, "Heat Transfer in the Boiling of Water on a Porous Surface in an Annular Channel," High Temp., **26**, pp. 712–717.
[13] Savkin, N. N., Kuzma-Kichta, Yu. A., and Komendantov, A. S., 1988, "Investigating Enhancement of Heat Transfer With Water Boiling Under Conditions of Forced Flow in a Tube With a Porous Coating," Therm. Eng., **35**, pp. 295–297.
[14] Zhang, L., Wang, E. N., Goodson, K. E., and Kenny, T. W., 2005, "Phase Change Phenomena in Silicon Microchannels," Int. J. Heat Mass Transfer, **48**, pp. 1572–1582.
[15] Kandlikar, S. G., Kuan, W. K., Willistein, D. A., and Borrelli, J., 2006, "Stabilization of Flow Boiling in Microchannels Using Pressure Drop Elements and Fabricated Nucleation Sites," ASME J. Heat Transfer, **128**, pp. 389–396.
[16] Koşar, A., Kuo, C.-J., and Peles, Y., 2005, "Boiling Heat Transfer in Rectangular Microchannels With Reentrant Cavities," Int. J. Heat Mass Transfer, **48**, pp. 4867–4886.
[17] Koşar, A., Kuo, C.-J., and Peles, Y., 2005, "Reduced Pressure Boiling Heat Transfer in Rectangular Microchannels With Interconnected Reentrant Cavities," ASME J. Heat Transfer, **127**, pp. 1106–1114.
[18] Kuo, C.-J., Koşar, A., Peles, Y., Virost, S., Mishra, C., and Jensen, M. K., 2006, "Bubble Dynamics During Boiling in Enhanced Surface Microchannels," J. Microelectromech. Syst., **15**, pp. 1514–1527.
[19] Kuo, C.-J., and Peles, Y., 2007, "Local Measurement of Flow Boiling in Structured Surface Microchannels," Int. J. Heat Mass Transfer, **50**, pp. 4513–4526.
[20] Kuo, C.-J., and Peles, Y., 2008, "Flow Boiling Instabilities in Microchannels and Means for Mitigation by Reentrant Cavities," ASME J. Heat Transfer, **130**, p. 072402.
[21] Jones, R., Pate, D., and Bhavnani, S., 2006, "Phase Change Thermal Transport in Etched Silicon Microchannel Heat Sinks," *Proceedings of the 13th International Heat Transfer Conference*, Sydney, Australia.
[22] Jones, R. J., Pate, D. T., and Bhavnani, S. H., 2007, "Control of Instabilities in Two-Phase Microchannel Flow Using Artificial Nucleation Sites," Technical Conference and Exhibition on Integration and Packaging of MEMS, NEMS, and Electronic Systems, Vancouver, Canada.
[23] Pate, D. T., Jones, R. J., and Bhavnani, S. H., 2006, "Cavity-Induced Two-Phase Heat Transfer in Silicon Microchannels," *Proceedings of the Tenth Intersociety Conference on Thermal and Thermomechanical Phenomena in Electronics Systems*, San Diego, CA, pp. 71–78.
[24] Webb, R. L., 1981, "The Evolution of Enhanced Surface Geometries for Nucleate Boiling," Heat Transfer Engineering, **2**, pp. 46–69.
[25] Steinke, M. E., and Kandlikar, S. G., 2004, "Control and Effect of Dissolved Air in Water During Flow Boiling in Microchannels," Int. J. Heat Mass Transfer, **47**, pp. 1925–1935.
[26] Chen, T., and Garimella, S. V., 2006, "Effects of Dissolved Air on Subcooled Flow Boiling of a Dielectric Coolant in a Microchannel Heat Sink," ASME J. Electron. Packag., **128**, pp. 398–404.
[27] Collier, J. G., 1981, *Convective Boiling and Condensation*, 2nd ed., McGraw-Hill, New York.
[28] Blevins, R. D., 1992, *Applied Fluid Dynamics Handbook*, Van Nostrand Reinhold Company, New York.
[29] Chisholm, D., and Sutherland, L. A., 1969, "Predictions of Pressure Gradients in Pipeline Systems During Two-Phase Flow," Symposium on Fluid Mechanics and Measurements in Two-Phase Flow Systems, University of Leeds.
[30] Mishima, K., and Hibiki, T., 1996, "Some Characteristics of Air-Water Two-Phase Flow in Small Diameter Vertical Tubes," Int. J. Multiphase Flow, **22**, pp. 703–712.
[31] Lockhart, R. W., and Martinelli, R. C., 1949, "Proposed Correlation of Data for Isothermal Two-Phase, Two-Component Flow in Pipes," Chem. Eng. Prog., **45**, pp. 39–48.
[32] Lee, J., and Mudawar, I., 2005, "Two-Phase Flow in High-Heat-Flux Micro-Channel Heat Sink for Refrigeration Cooling Applications: Part II—Heat Transfer Characteristics," Int. J. Heat Mass Transfer, **48**, pp. 941–955.
[33] Chen, T., and Garimella, S. V., 2006, "Measurements and High-Speed Visualizations of Flow Boiling of a Dielectric Fluid in a Silicon Microchannel Heat Sink," Int. J. Multiphase Flow, **32**, pp. 957–971.
[34] Yan, Y.-Y., and Lin, T.-F., 1998, "Evaporation Heat Transfer and Pressure Drop of Refrigerant R-134a in a Small Pipe," Int. J. Heat Mass Transfer, **41**, pp. 4183–4194.
[35] Lee, H. J., and Lee, S. Y., 2001, "Heat Transfer Correlation for Boiling Flows in Small Rectangular Horizontal Channels With Low Aspect Ratios," Int. J. Multiphase Flow, **27**, pp. 2043–2062.
[36] Bertsch, S. S., Groll, E. A., and Garimella, S. V., 2008, "Review and Comparative Analysis of Studies on Saturated Flow Boiling in Small Channels," Nanoscale Microscale Thermophys. Eng., **12**, pp. 187–227.
[37] Cooper, M. G., 1984, "Saturation Nucleate Pool Boiling—A Simple Correlation," First UK National Conference on Heat Transfer, University of Leeds, pp. 785–793.
[38] Cooper, M. G., 1984, "Heat Flow Rates in Saturated Nucleate Pool Boiling—A Wide-Ranging Examination Using Reduced Properties," Adv. Heat Transfer, **16**, pp. 157–239.
[39] Chen, J. C., 1966, "Correlation for Boiling Heat Transfer to Saturated Fluids in Convective Flow," I&EC Process Des. Dev., **5**, pp. 322–329.
[40] Hausen, H., 1943, "Darstellung des Wärmeüberganges in Rohren durch verallgemeinerte Potenzbeziehungen," Z. VDI-Beiheft Verfahrenstechnik, **4**, pp. 91–102.
[41] Jones, B. J., McHale, J. P., and Garimella, S. V., 2009, "The Influence of Surface Roughness on Nucleate Pool Boiling Heat Transfer," ASME J. Heat Transfer, **131**, p. 121009.
[42] Nishikawa, K., Fujita, Y., Ohta, H., and Hidaka, S., 1982, "Effect of the Surface Roughness on the Nucleate Boiling Heat Transfer Over the Wide Range of Pressure," *Proceedings of the Seventh International Heat Transfer Conference*, Müchen, Germany, Vol. 4, pp. 61–66.
[43] Nishikawa, K., Fujita, Y., Ohta, H., and Hidaka, S., 1982, "Effects of System Pressure and Surface Roughness on Nucleate Boiling Heat Transfer," Mem. Fac. Eng., Kyushu Univ., **42**(2), pp. 95–111.
[44] Gorenflo, D., 1993, *Pool Boiling*, VDI Heat Atlas, VDI Verlag, Düsseldorf, Germany.
[45] Lee, H. J., and Lee, S. Y., 2001, "Pressure Drop Correlations for Two-Phase Flow Within Horizontal Rectangular Channels With Small Heights," Int. J. Multiphase Flow, **27**, pp. 783–796.